Comparison of the properties of composition-tunable CdSe–ZnSe and $Zn_xCd_{1-x}Se$ nanocrystallites: Single- and double-pot synthesis approach

Himani Sharma [a,d], Shailesh N. Sharma [a,*], Sukhvir Singh [b], N.C. Mehra [c], Gurmeet Singh [d], S.M. Shivaprasad [a]

[a] Electronic Materials Division, National Physical Laboratory, Dr. K. S. Krishnan Marg, New Delhi 110 012, India
[b] Electron Microscope Section, National Physical Laboratory, Dr. K. S. Krishnan Marg, New Delhi 110 012, India
[c] USIC, University of Delhi, Delhi 110 007, India
[d] Department of Chemistry, University of Delhi, Delhi 110 007, India

ABSTRACT

In this work, a simple, effective and reproducible synthetic route (single-pot (SP) approach) for the preparation of high quality core–shell CdSe–ZnSe quantum dots without the use of any pyrophoric organometallic precursors is presented and their properties are compared with those prepared by the conventional double-pot (DP) approach. Effective surface passivation of stoichiometric, monodispersed, small-sized (∼5 nm) CdSe nanocrystallites is achieved by coating them with a ZnSe shell by single-pot approach. The resulting core–shell nanocrystallites exhibit high quantum yield values ∼11.33%, narrow line-width of the PL band, stable surface-bonds configuration and superior structural properties at lower Zn content (∼10 at.%). With increasing Zn content (≥20 at.%), a composition-tunable emission across the visible spectrum has been demonstrated by a systematic blue-shift in emission wavelength due to the formation of ternary $Zn_xCd_{1-x}Se$ quantum dots with acceptable luminescence properties. Here, contribution to emission process from surface states of nanocrystallites increases with zinc content. The core–shell and ternary QD's formed by different routes are modeled, based on the observations of several complimentary techniques (XPS depth-profiling, PL, UV–VIS absorbance, TEM/SAED). The improved properties of core–shell CdSe–ZnSe quantum dots with similar zinc content using single-pot synthesis approach as compared to the corresponding samples obtained by double-pot synthesis, is due to better-passivation effect rendered by thin ZnSe-shell in the SP approach. Their strong luminescence, narrow emission bands and wide colour-tunability makes such quantum dot structures attractive for various scientific and commercial applications.

1. Introduction

Colloidal semiconductor nanocrystals, also known as quantum dots (QDs) are of tremendous fundamental and technical interest owing to their applications as light-emitting devices, lasers and biological labels [1–4]. Among the various materials, colloidal CdSe QDs are the most sought ones, due to their tunable emission in the visible range [5,6].

The photoluminescence (PL) efficiencies of nanocrystals are known to be sensitive to the nature of the particle surface because of the large surface area and the presence of surface states caused by uncoordinated atoms [7]. Such surface states act as quenchers of luminescence, and thus the passivation of the surface bonds is the key to prepare semiconductor nanocrystals with high emission effi-

ciencies [7,8]. The judicious choice of a passivating agent can in fact improve the size-dependent band-edge luminescence efficiency, while preserving the solubility and processability of the particles. Such surface passivation has been achieved using organic capping agents (TOP, TOPO, etc.) as well as the formation of inorganic core–shell systems such as CdSe–ZnS, CdSe–ZnSe and CdSe–CdS [9–11]. However, inorganic-passivation of QDs can form core–shell structured nanocrystals (CdSe–ZnSe, CdSe–ZnS, CdSe–CdS) that are more robust than the organic-coated QDs, in terms of chemical degradation and photo-oxidation [12,13]. The major limitation of using inorganic-passivation is the lattice mismatch between the core and shell where the interface strain increases with increasing shell thickness and eventually relaxes by forming misfit dislocations, which consequently degrades the optical properties of QDs [8]. Thus, it is highly imperative to develop new synthesis methods or strategies to produce highly luminescent and stable core–shell semiconductor QDs. The recent approaches to synthesize luminescent nanocrystals with distinct core–shell–shell (CdSe–CdS–ZnS)

structure have not been successful in yielding core–shell nanocrystals with desirable properties [14]. For the CdSe–ZnSe system practically not much work has been done, whereas CdSe–ZnS and CdSe–CdS are the most intensively studied ones [12,13]. The advantage of using ZnSe is its lattice parameter mismatch with CdSe being smaller ~0.07 as compared to ZnS ~0.11, due to which interfacial defects, and non-radiative decay would be much less [15a]. Secondly, its band gap is wider (2.72 eV) than that of CdSe ($\sim$1.74 eV), a requisite condition for an effective confinement of electrons and holes within CdSe core [15a]. Though traditionally core–shell semiconductor QDs have been widely popular for their distinctive fluorescent properties, not much literature could be found on stiochiometric alloy nanoparticles which also show potential of unique tunable optical properties. Recent publications by Shuming Nie et al. [15b,c] have shown synthetic route to grow tunable ternary semiconductor alloys. Also extensive investigation has been done on thin film semiconductor alloys due to their wide application in optoelectronics, but only few studies have been reported for the preparation of alloy or composite nanocrystals synthesized by wet chemistry routes [16–18]. In this work, a simple single-pot synthesis procedure has been adopted to prepare both CdSe–ZnSe core–shell as well as $Zn_xCd_{1-x}Se$ ternary alloy nanocrystals systematic alloy varying the amounts of Zn-precursor. The results are compared with the corresponding samples obtained from conventional double-pot synthesis approach. It has been found that beyond an optimum amount of Zn (>20 at.%), there is a transition from core–shell (CdSe–ZnSe) with high PL efficiency and stability, to ternary ($Zn_xCd_{1-x}Se$) semiconductor nanocrystals with reasonably intense luminescence and stability. However, at very high concentrations of Zn ($\geq$40 at.%), the luminescence properties of $Zn_xCd_{1-x}Se$ nanocrystals deteriorate due to the marked effect of surface states or defect densities associated with higher amount of Zn incorporation in CdSe lattice. In the case of double-pot synthesis, although core–shell CdSe–ZnSe semiconductor nanocrystals are formed they exhibit inferior properties as compared to the corresponding one's obtained by single-pot synthesis.

2. Experimental

The synthesis of CdSe nanoparticles were carried out by the chemical route using TOP/TOPO capping method to control the growth of the nanoparticles to desired sizes, whose details can be found elsewhere [19,20]. The materials used were of the purest quality available and used as received. Cadminum oxide CdO (Aldrich, 99.99% purity), Tetradecyl phosphonic acid TDPA (Alfa Aesar, 98% purity), Trioctyl phosphine Oxide TOPO (Aldrich, 99% purity), Trioctyl phosphine TOP (Aldrich, 90% purity), Selenium powder (Aldrich, 99.5% purity) and Zinc acetate (Aldrich, 98% purity) were used. The product obtained by the solid state reaction was purified using a rigorous purification method of several steps. The washing was done with methanol as a solvent to ensure the complete removal of the unreacted precursors and other unwanted amorphous material. The nanocrystals were further isolated by centrifugation and decantation before filtering through a 0.1 μm filter. The recovered powder of nanocrystals was used to carry out XPS at every stage of the washing. Initial washing does indicate the presence of Cd-phosphonates which was evident from the careful analysis of the binding energy shifts in Cd and P core levels. The washing was repeated till no such shift in the binding energy was observed in XPS analysis, thus ruling out the presence of any unwanted amorphous material.

Absorption spectra were recorded using Shimadzu 3101 spectrometer. The PL was measured using a home assembled system consisting of a two stage monochromator, a photomultiplier tube (PMT) with a lock-in amplifier for PL detection, and an Ar+ ion laser operating at 488 nm and 5 mW (corresponding to 0.125 W cm^{-2}) power for excitation. X-ray photoelectron spectroscopy (XPS) measurements were performed in an ultra-high vacuum chamber (PHI 1257) with a base pressure of $\sim$4 × 10^{-10} Torr. The XPS spectrometer is equipped with a high resolution hemispherical electron analyzer (279.4 mm diameter with 25 meV resolution) and a Mg (Kα) ($h\nu$ = 1253.6 eV) X-ray excitation source.

2.1. Synthesis of CdSe–ZnSe core–shell and $Zn_xCd_{1-x}Se$ ternary alloy nanocrystals

Single-pot synthesis. Here zinc acetate was used as a zinc precursor and its amount was varied (from 0 to 50%) as per the molarity ratio of ZnSe/CdSe. Experimentally $Zn(Ac)_2$ + TDPA + CdO + TOPO were heated in a round bottom flask up to 300 °C in Ar atmosphere. This mixture was then cooled down to 275 °C and the solu-

tion of TOP-Se (TOP = 1.1 ml and Se 0.0254 g) was added drop wise. The temperature was maintained at 250 °C for few minutes before the mixture was cooled to room temperature to obtain the product.

Double-pot synthesis. For the post synthesis addition of $Zn(Ac)_2$, the method is a two step preparation technique in accordance with the usual procedure for the synthesis of CdSe–ZnSe core–shell nanocrystals [21].

First, the synthesis of standard CdSe nanocrystals ($\sim$Cd:Se-2:1) was done by the chemical route [19,20]. The second step has the following steps involved:

Solution A. In a beaker 1.5 ml of TOP + 0.0254 g of Se + 0.0884 g of $Zn(Ac)_2$ were heated under Ar atmosphere to dissolve Se and $Zn(Ac)_2$ in TOP. This solution was then stored under Ar atmosphere and sealed with a paraffin tape to avoid air contamination.

Solution B. In a separate round bottom flask, prepared CdSe 2:1 + 1.8884 g of TOPO and 0.116 g of TDPA were heated till 190 °C. At this temperature, solution A was added drop wise with continuous stirring. The addition was very slow and took nearly 40 min. This mixture was maintained at 190 °C for an hour before cooling down to the RT.

3. Results and discussion

The initial Cd/Se molar ratio and precursor concentrations are the key factors for obtaining luminescent and stable CdSe–ZnSe core–shell nanocrystals. In our earlier work, it was experimentally determined that the precursor ratio of 2:1 yielded smallest nanoparticles with highest luminescence and optimal stiochiometry between Cd and Se [20]. Thus for the synthesis of core–shell CdSe–ZnSe and ternary ($Zn_xCd_{1-x}Se$) semiconductor nanocrystals for both single- and double-pot synthesis methods, 2:1 CdSe system is chosen as the parent material. The properties i.e. optical gap, crystallite size determination by optical absorption, quantum yield values of CdSe nanocrystallites with different concentrations of Zn (at.%) are summarized in Table 1.

3.1. PL results

Fig. 1A (curves a–e) shows the absorption and photoluminescence spectra of CdSe nanocrystals synthesized with single-pot approach with different concentrations of Zn ranging from 0 to 50 at.%. The inset shows their corresponding colour photographs displaying wide spectral range of luminescence under 365 nm UV exposure. From Fig. 1A(a), corresponding to Cd/Se $\sim$ 2:1 (Zn $\sim$ 0 at.%), the sharp absorption features ($\lambda_{peak} \sim$ 500 nm) suggests monodispersity and the narrow PL emission ($\lambda_{peak} \sim$ 510 nm) indicates band-edge emission. The fact that the PL emission maximum lies close to its absorption-onset indicates that the PL emission arises as a result of direct recombination between LUMO and HOMO charge carriers [22]. This implies efficient passivation by TOP/TOPO groups, although weak signatures of surface states are evident by the presence of slight broad PL emission at λ > 600 nm. With the introduction of Zn $\sim$ 10 at.%, both absorption and PL spectra (Fig. 1A(b)) shows a red-shift as compared to the virgin CdSe–2:1 system (Fig. 1A(a)), with corresponding λ_{max} values being 519 and 540 nm, respectively. Such a red shift has been attributed to the partial leakage of the exciton into the shell in the past [10,15]. With the variation of Zn from 0 to 10 at.% both CdSe and core–shell CdSe–ZnSe QD's exhibit similar bright green luminescence (insets

Table 1
Summary of physical properties of core–shell CdSe/ZnSe and ternary ($Zn_xCd_{(1-x)}Se$) QDs.

Sample	Band gap (eV)	Size (nm) UV–Vis	Quantum yield (%)
CdSe~2:1	2.322	5.02	10.36
SP-10%	2.271	5.92	11.33
SP-20%	2.305	5.75	1.45
SP-40%	2.418	5.25	0.093
SP-50%	2.116	7.05	–
DP-10%	2.233	6.15	0.552
DP-20%	2.236	6.13	1.43
DP-40%	2.176	6.54	–
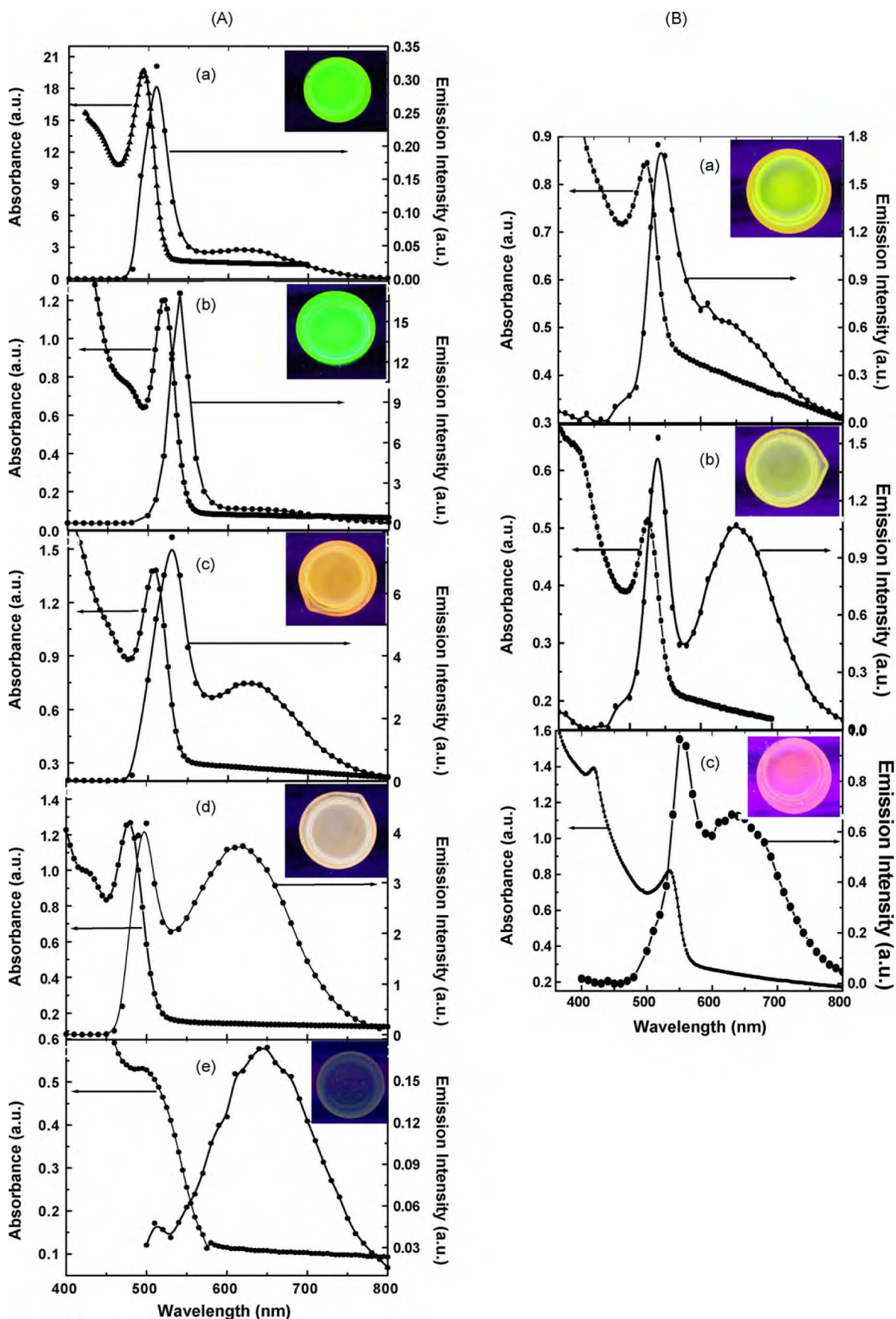
Fig. 1. Absorption and PL spectra of (A) SP synthesized core–shell CdSe–ZnSe and ternary $Zn_xCd_{1-x}Se$ QD's for varying concentrations of Zn; (a) 0 at.%; (b) 10 at.%; (c) 20 at.%; (d) 40 at.% and (e) 50 at.% and (B) DP synthesized core–shell CdSe–ZnSe QD's for varying concentrations of Zn; (a) 10 at.%; (b) 20 at.% and (c) 40 at.% respectively. The insets show the corresponding color photographs upon exposure to 365 nm UV lamp.

of Fig. 1A(a and b)). As shown in Fig. 1A(b), the formation of a core–shell (CdSe–ZnSe) structure results in an enhancement of PL by about 6 times with the overall shape of both absorption and PL spectra essentially remaining the same. Another noticeable feature is the complete absence of surface related states at $\lambda > 600$ nm indicating better surface passivation by ZnSe-shell in addition to TOP/TOPO groups. In addition, the linewidth of the PL peak remained essentially unchanged (FWHM ~ 36 nm) during core–shell formation, indicating that the CdSe nanocrystallites remained substantially monodispersed.

From Table 1, the quantum yield of core–shell (CdSe–ZnSe) for Zn ~ 10 at.% increases as compared to the core-CdSe (2:1) system which further indicates the formation of ZnSe shell on CdSe-core system. At the same time, the growth of the thin ZnSe-shell layers on CdSe-core resulted in a marginal increase of the average size of the nanocrystals from 5 to 5.75 nm (Table 1). However, upon further increase in the concentration of Zn ~ 20 at.%, both absorption ($\lambda_{peak} \sim 508$ nm) and PL spectra ($\lambda_{peak} \sim 530$ nm) (Fig. 1A(c)) shows a blue-shift with respect to the corresponding spectra of Zn ~ 10 at.% but still maintains a red-shift as compared to the corresponding spectra of core-CdSe(2:1) system ($\lambda_{Abs. Peak} \sim 500$ nm; $\lambda_{PLpeak} \sim 510$ nm) (Fig. 1A(a)). Here, the PL intensity (Fig. 1A(c)) although decreases as compared to Zn ~ 10 at.% case (Fig. 1A(b)) is slightly higher to the core-CdSe(2:1) system (Fig. 1A(a)) thus retaining core(CdSe)–shell(ZnSe) characteristics. The concomitant development of surface states at $\lambda > 580$ nm for core–shell system corresponding to Zn ~ 20 at.% is manifested as increase in FWHM (~ 53.8 nm) as compared to the CdSe-core system. As long as the strain can be tolerated, the ZnSe layer passivates the interface trap states and does not create additional mid-gap states. Once past a critical shell thickness, due to higher lattice-mismatch between ZnSe–CdSe layers, the strain is released through the formation of dislocations in the shell which act as non-radiative recombination centers and lowers the quantum yield as compared to lower Zn content case (~ 10 at.%). With further increase in Zn ~ 40 at.%, both absorption and PL spectra (Fig. 1A(d)) peak positions shift towards blue with respect to the corresponding spectra of Zn ~ 20 at.% (Fig. 1A(c)) with $\lambda_{Abs.max}$ and λ_{PLmax} values being ~ 476 and 509 nm, respectively. From Fig. 1A(d), the surface states ($\lambda_{PLmax} \sim 627$ nm) have a significant contribution, and its intensity is only marginally lower than the CdSe exciton PL peak (~ 509 nm). With the increase in Zn content from 20 to 40 at.%, the luminescence color changes from orange to peach (insets of Fig. 1A(c and d)). On comparison with CdSe-core system (Fig. 1A(a)), for Zn ~ 40 at.%, the absorption peak shows a significant blue-shift (from 500 to 476 nm) while PL peak position shows a marginal blue-shift of 1 nm (from 510 to 509 nm) and a reduction in intensity as well. Thus from Table 1, the lower quantum yield for Zn ~ 40 at.% as compared to CdSe-core system is due to the presence of higher defects because of higher Zn incorporation into the CdSe lattice with the resultant development of surface-states. At further higher Zn content (~ 50 at.%) (Fig. 1A(e)), there is a complete dominance of surface states ($\lambda_{PLmax} \sim 645$ nm) over CdSe exciton peak ($\lambda_{PLmax} \sim 509$ nm) in the PL spectrum and even the absorption peak is not distinct as compared to CdSe-core and lower Zn (10–40 at.%) samples. Thus beyond an optimum Zn content (10 at.%), due to the creation of a large number of defects at the core–shell interface because of the large lattice-mismatch between CdSe and ZnSe with increase in shell thickness, the optical properties of CdSe–ZnSe system shows a significant deterioration. In fact, the observed systematic composition-controlled shift of the absorption and emission maximum to shorter wavelength for Zn ≥ 40 at.% could be explained by the formation of ternary $Zn_xCd_{1-x}Se$ composite nanocrystals via intermixing wider band-gap ZnSe with the narrower band-gap CdSe nanocrystals rather than forming core–shell (CdSe–ZnSe) or separate CdSe and ZnSe nanoparticles respectively. If ZnSe

nanocrystals would have formed separately, the corresponding PL and absorption peaks should have appeared at energies higher than bulk band edge of ZnSe ~ 2.69 eV [23]. The absence of such individual peaks rules out the possibility of formation of ZnSe nanocrystals. On the other hand if the CdSe–ZnSe core–shell system were formed, the resulting absorption and emission maximum would have shifted to longer wavelength, as compared to core-CdSe (2:1) system as happened in the case of samples with Zn content varying from 10 to 20 at.% (Fig. 1A, curves b & c). Thus lower Zn content (10–20 at.%), initiates core–shell CdSe–ZnSe nanocrystals formation, whereas for higher Zn content (≥ 40 at.%), formation of ternary $Zn_xCd_{1-x}Se$ composite nanocrystals are favored. As evident from insets of Fig. 1(A), with increase in Zn content particularly for Zn > 20 at.%, the color uniformity decreases and quantum dots with color graded-shells are obtained.

From Table 1, there is no appreciable variation in the crystallite sizes (~ 5–6 nm) with increase in Zn concentration (0–50 at.%). This suggests that using single pot synthesis approach, we can tune the optical properties of core–shell CdSe–ZnSe for lower concentrations of Zn (≤ 20 at.%) and of ternary $Zn_xCd_{1-x}Se$ composite nanocrystals for higher concentrations of Zn (≥ 40 at.%) without much variation in the crystallite size.

Fig. 1B(a–c) shows the absorbance and PL spectra of Zn:CdSe samples synthesized by double-pot approach for different Zn content varying from 10 to 40 at.%. With increase in Zn content (10–40 at.%), both absorption and PL maxima shifts towards longer wavelength (red-shift) as compared to the core-CdSe (2:1) system indicating that the core–shell structure is still being formed. However, incomplete passivation with shell thickness for the largely mismatched core shell structures, the interface strain accumulates dramatically with increasing shell thickness and eventually can be released through the formation of misfit dislocations, degrading the optical properties. Even at lower concentration of Zn (~ 10 at.%), surface state contribution to PL (Fig. 1B(a)) is quite significant unlike in the case of corresponding sample synthesized by single-pot approach (Fig. 1A(b)). Thus, for the same concentration of Zn (~ 10 at.%), PL properties of SP sample are quite superior (less FWHM, high PL intensity, no surface state formation) as compared to the corresponding DP sample, although PL peak position is the same ~ 540 nm for both. Another interesting feature observed here is that for DP samples even at higher concentrations of Zn ~ 40 at.%, no signatures of formation of ternary $Zn_xCd_{1-x}Se$ composite nanocrystals are seen (i.e. no blue-shift in absorption and PL maxima with respect to CdSe-core) unlike in the case of corresponding SP samples. In the case of DP samples, the color of the PL as (shown by the insets of Fig. 1B), is normally dominated by broad deep trap emission and thus appears faint as compared to the intense band edge luminescence from the corresponding SP samples. The tendency of color-graded shells becomes prominent even at lower concentration of Zn ~ 10 at.% with color varying from yellowish green, light yellow and green with increase in Zn content from 10 to 40 at.% respectively (insets of Fig. 1B).

This marks the importance of single-pot synthesis approach where one can obtain both similar-sized (5–6 nm) CdSe–ZnSe core–shell and ternary $Zn_xCd_{1-x}Se$ composite nanocrystals with superior optical properties by simply varying the amount of Zn whereas in case of the double-pot synthesis approach, only CdSe–ZnSe core–shell systems are obtained with relatively more defects (surface states prominent) as compared to the former.

3.2. PL decay

Decay of PL intensity is a good indication of the instability of semiconductor nanocrystals particularly of the surface bond configurations [24,25]. The PL peak intensity was recorded for different times corresponding to wavelength of the peak of PL spec-
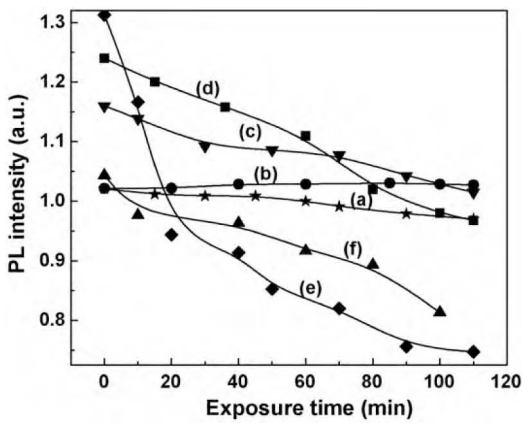
Fig. 2. PL decay of CdSe–ZnSe systems as a function of time of laser exposure for varying concentrations of Zn; SP (curves a–e; Zn ~ 0, 10, 20, 40 and 50 at.%) and DP (curve f; Zn ~ 10 at.%) respectively.

trum. In Fig. 2, decay of the PL intensity at the peak wavelength due to exposure to the laser radiation for CdSe-core, CdSe–ZnSe core–shell and ternary $Zn_xCd_{1-x}Se$ alloys formed by varying the Zn content (0–50 at.%) using single-pot synthesis approach are compared. For CdSe-core, CdSe–ZnSe core–shell systems, no PL decay was observed for lower Zn content (0–10 at.%) (Fig. 2(curves a and b)) and relatively less PL decay was noted for Zn ~ 20 at.% (Fig. 2(curve c)). However, a significant decay is observed only for ternary $Zn_xCd_{1-x}Se$ alloys with the rate of decay being dependent on the concentration of Zn (≥40 at.%) Fig. 2(curves d and e). For CdSe–ZnSe core–shell QD's using double-pot synthesis approach for Zn ~ 10 at.%, a considerable PL decay (Fig. 2, curve f) occurs with laser exposure, contrary to what obtained for the corresponding SP sample. To ensure the reproducibility of this PL decay, measurements were done repeatedly and for several hours and the PL decay trend was found to be the same. The above results suggest the formation of stable surface bonds in correlation with superior mechanical stability of the core–shell CdSe–ZnSe system synthesized by single-pot approach as compared to the corresponding core–shell sample synthesized by double-pot approach with similar Zn content (~10 at.%).

3.3. TEM results

Fig. 3A(a) shows a TEM bright field micrograph of core-CdSe(2:1) system along with corresponding SAED pattern as an inset. The micrograph exhibits a compact and dense structure of fine particles of spherical shape of about 40 nm in average size with tendency of agglomeration. This size significantly deviates from the particle size of 5 nm as calculated from the optical data (Table 1). However, further magnified area of the selected portion of Fig. 3A(a) (inset on the left side) reveals that a typical nanosized CdSe growth island is in fact a cluster of several smaller nanocrystals (size ~4–6 nm) each surface passivated by TOP/TOPO groups. Due to extremely small dimensions and high surface energy these nanocrystallites aggregate to give a resultant average size of 40 nm. It is not possible for the particles with 40 nm size to exhibit quantum confinement effect (E_g ~ 2.32 eV) since the optical properties of CdSe would become bulk-like (E_g ~ 1.74 eV) for the particle sizes much bigger than 4.9 nm (Bohr radius of CdSe exciton). Thus, for the CdSe-2:1 system, the size of the smaller CdSe nanocrystals as observed from the micrograph in the range of 4–6 nm, which is in good agreement with the optical absorption results. The corresponding SAED pattern which depicts a halo but with the ring patterns from the randomly oriented crystallites of nanometric dimensions also supports this.

Fig. 3A(b) shows an electron micrograph corresponding to the CdSe–ZnSe core–shell system for Zn ~ 10 at.%. The TEM depicts the agglomeration of round shaped particles with an average size of the particles being ≈12 nm. Some very fine particles of an average size of 5–6 nm clustered together are also seen as indicated by an arrow in Fig. 3A(b). Moreover, the density of nanoparticles is quite large as compared to the core-CdSe (2:1) system (Fig. 3A(a)). The corresponding SAED pattern (inset of Fig. 3A(b)) shows the presence of diffused rings revealing the presence of nanometric sized particles.

Fig. 3A(c) shows an electron micrograph corresponding to the CdSe–ZnSe core–shell system for Zn ~ 40 at.%. At this concentration of Zn, dual phase i.e. monodispersive and agglomerated phases are observed as depicted in the electron micrographs (Fig. 3A(c)). In one phase, particles of round head-shaped (size varying from 10 to 30 nm) with tailing morphology are observed, having an almost monodispersed distribution as indicated by the left portion of Fig. 3A(c). The corresponding ED pattern (inset of left portion of Fig. 3A(c)) shows the presence of distinct rings indicating a random distribution of fine grains. However, the right portion of Fig. 3A(c) shows typical fused bunches of nanocrystals with significant gap between two nanocrystallites. The corresponding ED pattern (inset of right portion of Fig. 3A(c)), exhibits well-defined rings with spotty features indicating randomly oriented large crystallites as a result of coalescence of smaller crystallites. Thus at a typical concentration of Zn ~ 40 at.%, co-existence of both core–shell (CdSe–ZnSe) and ternary $Zn_xCd_{1-x}Se$ nanocrystallite systems are indicated from both PL and TEM results.

At further higher concentration of Zn ~ 50 at.%, the ternary $Zn_xCd_{1-x}Se$ nanocrystallite systems are marked by a needle-shaped morphology (Fig. 3A(d)). Here, presence of distinct voids of different sizes are also observed (Fig. 3A(d)). Such needle-shaped morphology of the particles is often seen in the case of ZnO quantum dots [26]. The presence of higher unpassivated zinc concentration makes the nanocrystallite highly susceptible to oxidation, rendering the core–shell quantum dot defective. The diffused and weak rings as shown by the corresponding diffraction pattern (inset on right of Fig. 3A(d)) also indicates the formation of ZnO or/and SeO_3 species.

Fig. 3B(a and b) shows a TEM micrographs of CdSe–ZnSe core–shell system of DP sample (Zn ~ 10 and 40 at.%) along with their corresponding SAED patterns. Here, round-shaped particles (average size ~5–6 nm) exhibit higher agglomeration tendency as compared to the corresponding SP sample. The agglomeration tendency increases with increase in Zn content (10–40 at.%) (Fig. 3B(a and b)). The diffraction rings are indexed to the (1 0 1) & (1 0 2) planes of CdSe and (1 1 2) planes of ZnSe hexagonal systems respectively [27].

3.4. XRD results

The crystallographic properties of CdSe-core and CdSe–ZnSe systems corresponding to Zn ~ 10 at.% prepared by both SP and DP methods have been investigated by X-ray diffraction and are shown in Fig. 4 (curves a–c). As shown in Fig. 4(a), the typical planes of CdSe bulk system indexed as (1 0 1), (1 0 2) and (1 1 1) confirm the wurtzite phase of CdSe [27]. Here, the crystallnity of the nanoparticles is usually evidenced by the sharp XRD peaks (Fig. 4). As evident from Fig. 4 (curves a–c), the peaks at lower angles are the envelope of several reflections which provides further confirmation for the narrow size distribution of the particles. From the XRD patterns, the broadening of these diffraction peaks indicates that CdSe crystallites are nanometric in dimensions. The XRD patterns show mainly a large hump in the low angle region, that is characteristics of the general amorphous structure indicating the nanometric dimensions. As shown in Fig. 4(curves b and c), for CdSe–ZnSe core–shell systems prepared by SP and DP methods, the diffrac-
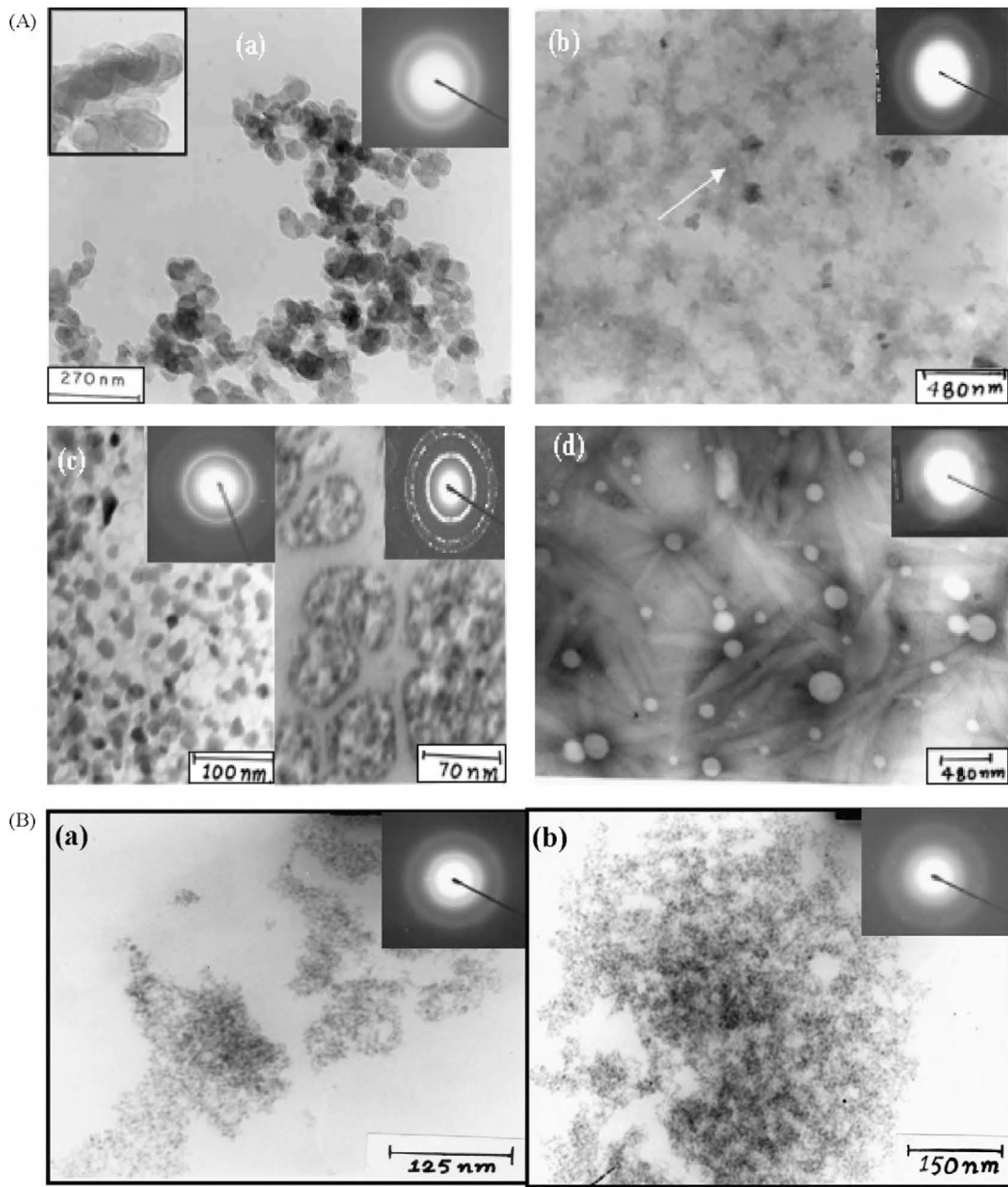
Fig. 3. TEM micrographs and the corresponding ED patterns (as inset) of CdSe–ZnSe systems for varying concentrations of Zn; (A) SP (a–d; Zn ∼ 0, 10, 40 and 50 at.%) and (B) DP (a, b; Zn ∼ 10 and 40 at.%) respectively. The inset on the left hand side of A(a) represents the magnified portion of the selected area.

tion patterns shift gradually to high reflection angles and 2θ values are much closer to bulk ZnSe than to bulk CdSe reflecting the compression of lattice plains of CdSe core [14]. This trend is prominent for SP sample as compared to DP sample. While ZnSe exists either as zinc-blende or as wurtzite in structure, it is expected that the core wurtzite CdSe will template the growth crystal structure for the ZnSe causing it also to go wurtzite. However, a comparison of the bulk lattice parameters shows that ZnSe is 7% shorter in bond length which would be a source of interfacial strain at the surface of the material [15a]. This strain can be imagined to exert itself upon the core QD and may be the basis for the increased stokes shift for SP samples as compared to the corresponding DP samples. Similar trend was also reported by Dabbousi et al. [13] on the growth of core/shell nanoparticles. Another noticeable feature observed in the XRD pattern is the slight peak broadening upon the shell addition as compared to CdSe-core thus supporting the core–shell formation by both SP and DP methods respectively (Fig. 4, curves

a–c). As estimated from Scherrer's formula, the average sizes of the CdSe–ZnSe nanocrystallites were found to be 5.0, 6.0 and 8.0 nm corresponding to Zn ∼ 0 and 10 at.% prepared by SP and DP methods respectively. The average sizes of CdSe–ZnSe nanocrystallites are in good agreement with optical data and TEM results.

A non-linear relationship was observed when the band gap energies of both bulk and nanocrystal $Zn_xCd_{1-x}Se$ were plotted against the Zn mole fractions. The modulation of the bandgap energy from linear dependence is known as band gap bowing effect and has been generally observed in compound semiconductor ternary alloys [28]. The nonlinearity can be expressed as a function of composition;

$$E_g(x) = E_{CdSe} + (E_{ZnSe} - E_{CdSe} - b)x + bx^2 \qquad (1)$$

where $E_g(x)$, E_{CdSe} and E_{ZnSe} are the energy gaps for the $Zn_xCd_{1-x}Se$ alloy, pure CdSe and ZnSe with x being the composition of Zn and b is the bowing parameter. The bandgap bowing
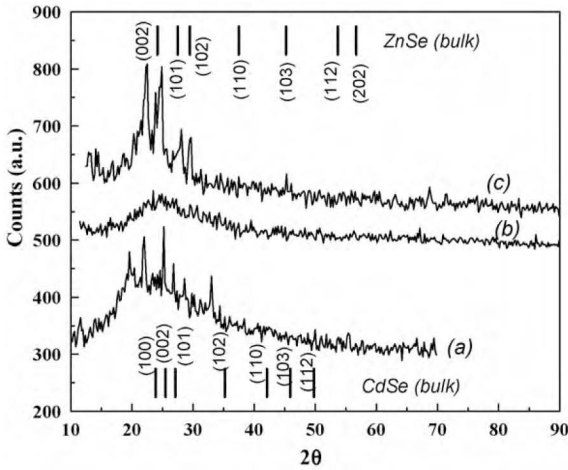
Fig. 4. XRD patterns of CdSe–ZnSe systems for varying concentrations of Zn; SP ((a) and (b); Zn ~ 0 and 10 at.%) and DP ((c); Zn ~ 10 at.%) respectively.
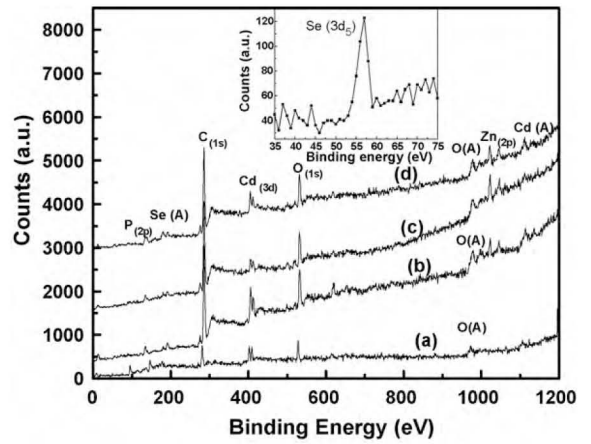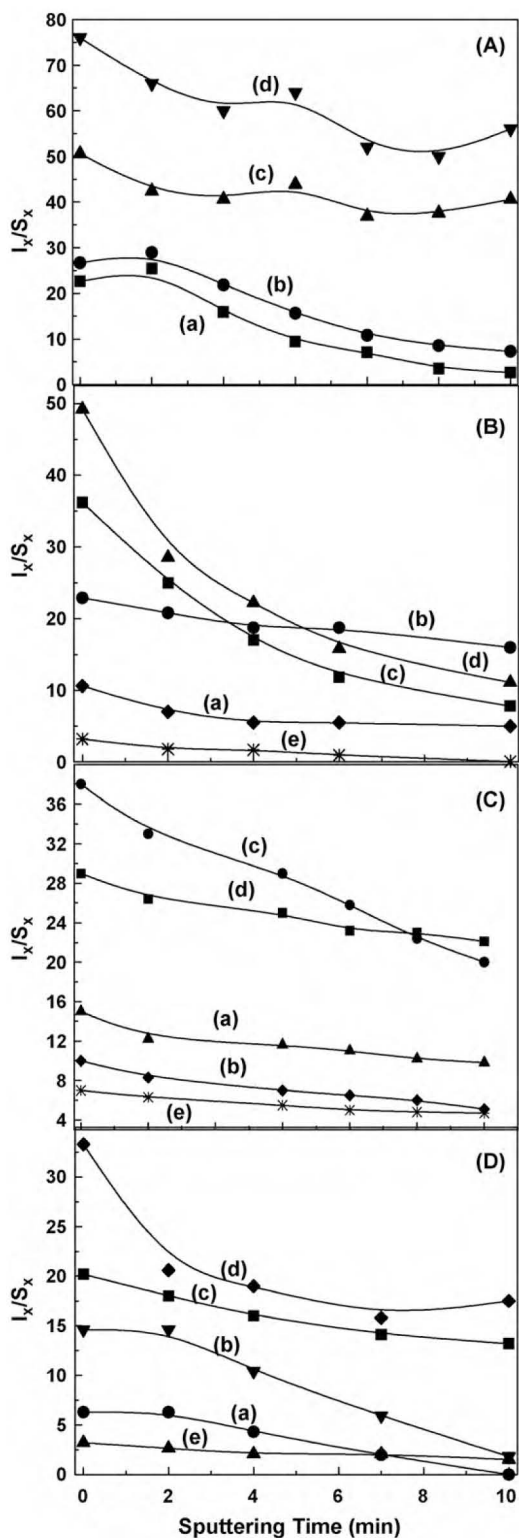

Fig. 5. XPS survey spectra of CdSe–ZnSe systems for varying concentrations of Zn; SP (a–c; Zn ~ 0, 10 and 40 at.%) and DP (d; Zn ~ 10 at.%) respectively.

parameter for a mixed crystal is composition dependent when two end-members (CdSe and ZnSe) have different lattice constants and depends on the fluctuations in the crystal field induced by the inter-substitutional atoms or rather than the structural disorder [29]. The bandgaps for ZnSe and CdSe in hexagonal (wurtzite) phases at $T = 60$ K are approximated as 2.86 and 1.84 eV respectively. The resulting composition dependent bandgaps for the hexagonal phases are then expressed as:

$$E_g(x) = 1.84 + (1.02 - b)x + bx^2 \qquad (2)$$

Among the various reported bowing parameters for the ZnSe and CdSe in the hexagonal (wurtzite) phase, the recent consensus appears to be that $b \sim 0.45$ independent of temperature [30,31]. For sample SP-50% ($Zn_xCd_{1-x}Se$); $x \sim 0.5$ and $E_g(x) \sim 2.116$ eV upon substituting these values along with $b \sim 0.45$ in Eq. (2) yields the quadratic equation in x yielding $x \sim 0.39$. Thus $x \sim 0.39$ is real value of x for the sample SP-50% i.e. ($x \sim 0.5$) with $Zn_xCd_{1-x}Se$ composition and these values agree fairly well within the limits of experimental error. Even for maximum value of $x \sim 0.5$, from Eq. (2), bowing parameter of $b \sim 0.9$ eV which is still quite small >1.0 eV as compared with those of other mixed crystals [32] which indicates that ZnSe and CdSe have a good miscibility [33]. Eq. (1) is valid mainly for ternary alloys as incorporating the value of $b \sim 0.45$, $E_g(x) \sim 2.418$ eV for sample SP-50% in Eq. (1) yields $x \sim 0.664$ which is absurd. This can be understood from the fact that at Zn ~ 40%, both core–shell (CdSe–ZnSe) and ternary alloys $Zn_xCd_{1-x}Se$ co-exist and as such Eq. (1) cannot be used to determine the value of x for core–shell quantum dots.

3.5. XPS results: general scan and depth profiling

In order to further examine the chemical composition, stoichiometric and bonding changes in core-CdSe (2:1), core–shell CdSe–ZnSe and ternary $Zn_xCd_{1-x}Se$ nanocrystallite CdSe systems with varied Zn content (0–40 at.%), the XPS survey spectra were obtained and are shown in Fig. 5. As shown in Fig. 5 (curves a–d), the presence of Cd $3d_{5/2}$ peak at ~405 eV indicates that Cd exists either in metallic form (i.e., unreacted Cd) or in CdSe form [34]. From the core-level profiles (figure not shown here), it is interesting to note that for CdSe nanocrystallite system, with the increase in Zn content (0–10 at.%), the broadness of the Cd-core levels i.e. full width at half maximum (FWHM) remains same while for higher Zn content ~40 at.% (i.e. for ternary $Zn_xCd_{1-x}Se$ alloy) and DP sample (Zn ~ 10 at.%), it increases which indicates that the effect of oxidation is prominent for ternary alloys and DP sample. However,

from Fig. 5, no splitting of the Cd 3d doublet was found which indicates that only Cd (from CdSe) is present on the surface and by XPS there is no evidence for CdO formation. Similarly, from Fig. 5 (curves a–d), the presence of Se 3d binding energy at ~55.5 eV (the inset represents the magnified portion) further confirms the presence of CdSe phase only [34]. From Fig. 5, the signatures of P XPS signal (~133 eV), C XPS signal (~282-286 eV) and Auger signal (~980 eV), O XPS signal (531 eV), Cd Auger signal (~620 eV) and Zn XPS signal (~1020 eV) [20,34,35] are also indicative of CdSe system with varied Zn content (0–40 at.%) and DP sample (Zn ~ 10 at.%). The presence of C, P and O comes from TOP/TOPO group indicating the presence of organic TOPO as a passivating layer. It is also worth noting that with the increase in Zn content from 0 to 40 at.%, the corresponding Zn signal ~1020 eV increased accordingly (Fig. 5, curves b–d).

Fig. 6 shows the XPS depth profiles of Cd, Se, O, P and Zn as a function of ion sputtering time for core-CdSe (2:1) (Zn ~ 0 at.%), core–shell CdSe–ZnSe (Zn ~ 10 at.%) and ternary $Zn_xCd_{1-x}Se$ (Zn ~ 40 at.%) alloy systems synthesized by single-pot approach. For comparison core–shell CdSe–ZnSe (Zn ~ 10 at.%) synthesized by double-pot approach is also given (Fig. 6(D)). The studies reveal the internal stoichiometry as the material is eroded layer by layer. In case of the core-CdSe (2:1) system, from Fig. 6(A), the similarity in the sputtering depth profiles of Cd and Se indicates the homogeneity along the depth i.e. stoichiometry for core-CdSe (2:1) system. Here, both Cd and Se are being sputtered together as CdSe species as a whole and not as Cd and Se separately. The relatively narrow shape of the Cd and Se sputtering profiles (0–2 min) indicates smallest size (~5 nm) of CdSe nanoparticle associated with core-CdSe (2:1) system. The similarity in the sputtering depth profiles of O and P shows efficient passivation of CdSe nanocrystallites achieved by TOP/TOPO groups with almost no trace of any oxidation of either Cd or Se atoms for core-CdSe (2:1) system.

Fig. 6(B) shows the depth-profile of various constituents of core–shell CdSe–ZnSe system corresponding to Zn ~ 10 at.%. The rapid drop in Zn signal strength during the initial stages of sputtering indicate the absence of any atomic Zn inside the core. This observation reiterates the fact that a very thin layer of ZnSe acts as an efficient and stable shell to CdSe. The initially higher concentration of Se signal intensity as compared to Cd is due to the presence of Se as ZnSe in the shell. However upon depth profiling, Se-related signal gradually decreases and follows the same trend as that of the Cd-related XPS signal. The initially higher concentration of O and P-signal intensities shows the presence of TOP/TOPO groups efficiently passivating the CdSe-core system.

Fig. 6. XPS depth profiles of core levels (a) Cd (3d) core; (b) Se (3d) core; (c) P (2p) core O (1s) and (e) Zn (2p) core of CdSe–ZnSe systems for varying concentrations of Zn; SP (A–C; Zn ∼ 0, 10 and 40 at.%) and DP (D; Zn ∼ 10 at.%) respectively.

Fig. 6(C) shows the XPS depth-profiles of Cd, Se, O, P and Zn elements for ternary $Zn_xCd_{1-x}Se$ alloy system (Zn ∼ 40 at.%). The similarity in the depth profiles of Cd, Se and Zn shows the presence of mainly ternary $Zn_xCd_{1-x}Se$ alloy at higher concentration of Zn ∼ 40 at.% rather than individual ZnSe or CdSe systems. The initial higher concentration of P- and O-related XPS signals shows

the presence of TOP/TOPO groups outside the ternary alloy system. However upon sputtering, the O-XPS signal decreases marginally and is almost constant while the P-related XPS signal decreases significantly indicating the absence of TOP/TOPO groups inside the ternary alloy system. The significant presence of oxygen even inside the core–shell nanocrystallite system is attributed to the higher defect density in higher zinc content (∼40 at.%) systems. The higher zinc (≥40 at.%) induced defect density is thus responsible for oxidation effects and eventually leading to deterioration of optical and structural properties of ternary $Zn_xCd_{1-x}Se$ alloy nanocrystallite systems.

Fig. 6(D) shows the XPS depth-profiles of Cd, Se, O, P and Zn elements for core–shell CdSe–ZnSe nanocrystallite synthesized with double-pot approach corresponding to Zn ∼ 10 at.%. Here, the Zn-signal decreases slightly upon sputtering and the signal remains steady throughout the depth profile indicating presence of Zn not only as ZnSe as a over-lying shell but also inside the CdSe-core itself unlike in the case of corresponding core–shell CdSe–ZnSe system (Zn ∼ 10 at.%) using SP approach (Fig. 6(B)). Though the similar sputtering depth-profiles of Cd- and Se- shows the presence of CdSe together inside the core, the initial higher concentration of Se as compared to Cd could be due to Se present as ZnSe as a shell on the core-CdSe (2:1) system. Here, the O-XPS signal upon depth profiling decreases steadily but the rate of decay in O-signal is higher in corresponding SP sample as compared to DP sample indicating substantial presence of O-inside the CdSe-core in DP sample leading to deterioration in its properties. This is further clear from the sputtering depth-profile of P which almost remains steady throughout, indicating TOPO's presence outside the shell and within the CdSe-core as well.

3.6. The model

On the basis of the complementary results of PL and its decay, UV–VIS absorption, TEM/TED and XPS (core-level and depth profiling), we propose a model for our nanocrystalline core-CdSe (2:1), core–shell CdSe–ZnSe and ternary $Zn_xCd_{1-x}Se$ alloy systems with varied amounts of Zn (∼0–50 at.%) using single-pot approach as shown in Fig. 7(A). Fig. 7(B) shows a schematic model for core–shell CdSe–ZnSe corresponding to Zn ∼ 10 and 40 at.% prepared using double-pot approach. Using single-pot approach with varied amounts of CdSe/ZnSe, CdSe-core, core–shell CdSe–ZnSe nanocrystallites having different shell (ZnSe) thicknesses were obtained up to Zn ∼ 0–20 at.% and for Zn ≥ 40 at.%, ternary $Zn_xCd_{1-x}Se$ alloys are obtained and the corresponding models are represented pictorially (Fig. 7A(a–e)). For core-CdSe (2:1) system, the smallest nanoparticle (size ∼ 5 nm) comprising of stiochiometric CdSe is obtained with no free/floating Cd or Se, as confirmed by XPS. Here, most of the TOPO is bounded to CdSe crystallites within the CdSe core (Fig. 7A(a)). Fig. 7A(b) corresponds to a typical core–shell CdSe–ZnSe system (Zn ∼ 10 at.%), where several CdSe grains are enclosed inside a CdSe nanoparticle with TOPO as the capping agent attached to Zn (of thin ZnSe shell) through O. Since there is no free Cd or Se available, as all Cd is attached to Se within the CdSe-core and the remaining Se atoms are attached to Zn forming a thin shell of ZnSe, thus ensuring a complete passivation of core-CdSe. Thus for a minimum concentration of Zn ∼ 10 at.%, the resulting core–shell nanocrystallite exhibits the following features: higher PL intensity (Q.Y.) values even being higher ∼11.33% than standard dye-Rhodamine 6G, narrow FWHM of the PL band, devoid of any surface-state formation and bestowed with stable surface bonds (no PL decay upon exposure to laser) and ability to withstand higher stress/strain values which renders it better than the parent core-CdSe(2:1) system. With increase in Zn content ∼20 at.%, the ZnSe-shell thickness increase is depicted in Fig. 7A(c). This leads to larger lattice-mismatch between ZnSe-shell and CdSe-
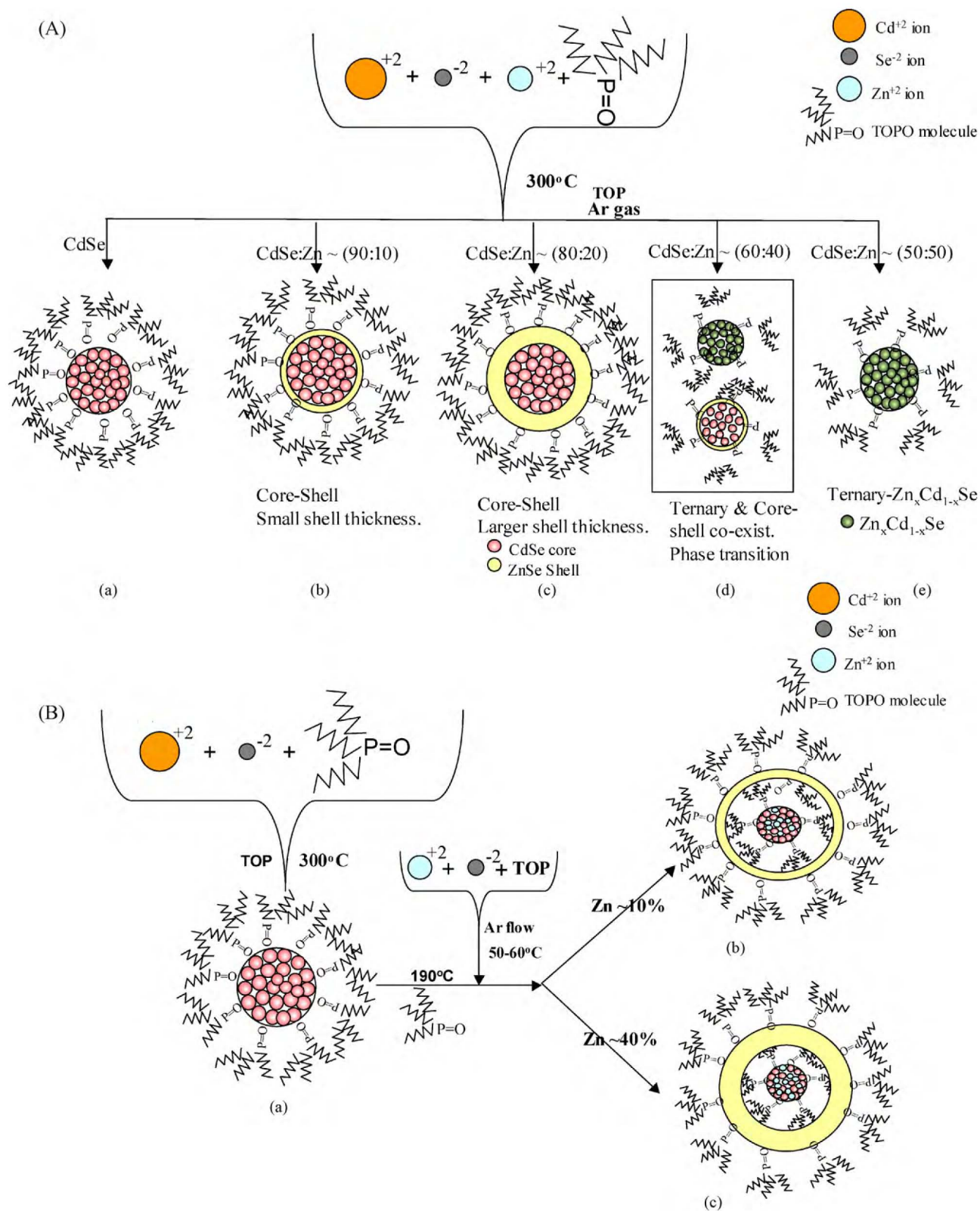
Fig. 7. Model of CdSe–ZnSe systems for varying concentrations of Zn; (A) SP; (a–e; Zn ~ 0, 10, 20, 40 and 50 at.%) and (B) DP; (a–c; Zn ~ 0, 10 and 40 at.%) respectively. Here, Zn ~ 0 at.% represents CdSe-core synthesized by single-pot method only.

core resulting in deterioration of structural and optical properties. With further increase in Zn ~ 40 at.%, the resulting nanocrystallite system is mainly ternary $Zn_xCd_{1-x}Se$ along with the presence of CdSe-core (Fig. 7A(d)). Here, a thin ZnSe shell is still being formed along with the diffusion of Zn inside the CdSe-core, leading to inter-

stitial voids within CdSe lattice thus resulting in inferior properties. The prominence of surface states here is due to higher ZnSe shell thickness which leads to higher lattice-mismatch and facilitates inter-diffusion of Zn as compared to the corresponding sample with Zn ~ 20 at.%. The fact that at Zn ~ 40 at.%, instead of adding

to the shell thickness, the nanocrystallite size slightly decreases as compared to Zn ~ 20 at.% case is a further testimonial for the formation of thin shell of ZnSe and diffusion of Zn into the CdSe-lattice. The dual-phase morphology depicted by TEM micrographs (Fig. 3(c)) also clearly points towards the simultaneous existence of both ternary $Zn_xCd_{1-x}Se$ and core–shell CdSe–ZnSe systems for Zn ~ 40 at.%. However, upon further increase in Zn ~ 50 at.%, the nanocrystallite system is devoid of any thin layer of ZnSe-shell and CdSe-core and only ternary $Zn_xCd_{1-x}Se$ alloy system is formed as represented pictorially by Fig. 7A(e). Higher incorporation of Zn into the CdSe-lattice results in the formation of higher defect density and the PL properties are being dictated by surface states only.

Fig. 7B (b and c) depicts the pictorial representation of formation of core–shell CdSe–ZnSe nanocrystallite system with Zn ~ 10 and 40 at.% from the parent core-CdSe (2:1) system (Fig. 7B(a)) using double-pot synthesis approach. As shown in Fig. 7B, upon addition of solution A and solution B and thereafter maintaining it at 190 °C for an hour before cooling it down to RT, CdSe-core with thin layer of CdSe-shell is being formed corresponding to Zn ~ 10 at.% (Fig. 7B(b)). However, here the shell thickness is thicker than that of the corresponding SP sample and hence the difference in properties. The presence of extra Zn inside the CdSe core, as elucidated by XPS is also shown in Fig. 7B(b). The diffusion of Zn inside the CdSe-core further increases along with increased shell thickness at higher concentration of Zn ~ 40 at.% as depicted in Fig. 7B(c). Therefore, after ZnSe-shell growth on CdSe-core nanocrystals, imperfection between core and shell might be induced due to surface reconstruction and lattice mismatch resulting in creation of vacancies [36]. These vacancies may provide an effective diffusion path for Zn from the shell into the CdSe-lattice thus leading to its inferior properties as compared to the corresponding SP sample. Here, TOPO/TOP species is being attached not only to core-CdSe but also to ZnSe-shell indicated from the steady P-depth profile data.

In summary, core–shell CdSe–ZnSe nanocrystallites can be formed with two different procedures: one-pot synthesis and two-pot synthesis. One-pot coating synthesis on the CdSe QDs is a new method which is achieved in a single step including the formation of CdSe QDs. Upon comparison of one-pot and two-pot synthesis method, the core–shell CdSe–ZnSe QDs synthesized with one-pot showed extremely high quantum yield ~11.33 higher than that of standard Rhodamine 6G dye. One can even see the bright fluorescence under ambient room light. The reason for the striking increase of quantum yield in comparison to two-pot synthesis can be attributed to the instant formation of ZnSe-shell right after core-CdSe (2:1) QDs growth ends. This reduces the chances of surface defects between CdSe and ZnSe. In case of two pot synthesis, the CdSe-core is already formed and the surface is capped by TOPO/TOP species in the first pot. In the second pot (ZnSe-shell coating), the formation of ZnSe layer could enclose some TOPO/TOP which forms a gap between core-CdSe and shell-ZnSe resulting in creation of defects.

It has been generally observed that for the synthesis of $Zn_xCd_{1-x}Se$ nanocrystals, a large excess of Se-precursor was used to prepare the starting CdSe QD's for a Se-rich surface [12]. This would aid the initial epitaxial growth of a thin shell of ZnSe which can alloy simultaneously with the CdSe QD's at high temperatures [12,37]. However, in our case, stoichiometric CdSe QD's were utilized for the synthesis of core–shell CdSe–ZnSe and ternary $Zn_xCd_{1-x}Se$ nanocrystals of similar nanocrystallite sizes whose optical properties can be tailored in the visible range by varying the concentration (x) of Zn. The use of stoichiometric QD's for the development of core–shell and ternary quantum dots by SP method have been reported for the first time to the best of author's knowledge.

4. Conclusions

An effective, simple and reproducible single-pot (SP) synthetic method has been developed for the formation of highly luminescent, stable and composition-tunable core–shell CdSe–ZnSe at lower zinc content and ternary $Zn_xCd_{1-x}Se$ semiconductor nanocrystallites with acceptable luminescence properties at higher zinc content. The emission wavelength across the visible spectrum can be tuned by merely varying the Zn content in core–shell and ternary quantum dots without much variation in the crystallite sizes. The core–shell CdSe–ZnSe semiconductor nanocrystallites formed by single-pot approach are superior to CdSe–ZnSe nanocrystallites formed by double-pot approach for the same concentration of Zn ($\geq$20 at.%). The improved properties (high quantum yield 11.33% narrow FWHM of the PL band ~29 nm, no PL-decay, ability to withstand higher stress/strain, superior structural properties as elucidated by TEM & TED results) are attributed to single-pot synthesis approach where formation of ZnSe-shell takes place immediately after the formation of core-CdSe resulting in relatively less surface-defects as compared to the corresponding sample prepared by double-pot synthesis. Moreover, by varying zinc content, using single-pot approach, one can form both core–shell and ternary quantum dots which is not so in the case of double-pot synthesis approach where only core–shell CdSe–ZnSe QD's are formed but with inferior properties as compared to corresponding single-pot samples. On the basis of results of XPS (core-level data and from depth-profiling measurements using Ar beam as a source of sputtering), PL, UV-VIS absorbance, TEM, TED and XRD, we formulate a model for our core–shell CdSe–ZnSe and ternary $Zn_xCd_{1-x}Se$ quantum dots synthesized by single- and double-pot approaches respectively.

References

[1] Yuji Araki, Koji Ohkuno, Takeshi Furukawa, Junji Saraie, J. Crystal Growth 301–302 (2007) 809.
[2] KippenyF T.C., M.J. Bowers II, A.D. Dukes III, J.R. McBride, R.L. Orndorff, M.D. Garrett, S.J. Rosenthal, J. Chem. Phys. 128 (2008) 084713.
[3] S. Mahapatra, T. Kiessling, E. Margapoti, G.V. Astakhov, W. Ossau, L. Worschech, A. Forchel, K. Brunner, J. Crystal Growth 301–302 (2007) 310.
[4] M. Han, X. Gao, J.Z. Su, S. Nie, Nat. Biotechnol. 19 (2001) 631.
[5] A.P. Alivisatos, W. Gu, C. Larabell, Annu. Rev. Biomed. Eng. 7 (2005) 55.
[6] M.L. Steigerwald, L.E. Brus, Acc. Chem. Res. 23 (1990) 183.
[7] L. Qu, X. Peng, J. Am. Chem. Soc. 124 (2002) 2049.
[8] I. Mekis, D.V. Talapin, A. Kornowski, M. Haase, H. Weller, J. Phys. Chem. B 107 (2003) 7454.
[9] D. Zhao, Z. He, W.H. Chan, M.M.F. Choi, J. Phys. Chem. C 113 (2009) 1293.
[10] Sung Jun Lim, Bonghwan Chon, Taiha Joo, Seung Koo Shin, J. Phys. Chem. C 112 (6) (2008) 1744.
[11] X. Chen, Y. Lou, C. Burda, Int. J. Nanotechnol. 1 (2004) 105.
[12] X. Peng, M.C. Schlamp, A.V. Kadavanich, A.P. Alivisatos, J. Am. Chem. Soc. 119 (1997) 7019.
[13] B.O. Dabbousi, J. Rodriguez-Viejo, F.V. Mikulec, J.R. Heine, H. Mattoussi, R. Ober, K.F. Jensen, M.G. Bawendi, J. Phys. Chem. B 101 (1997) 9463.
[14] D.V. Talapin, I. Mekis, S. Gotzinger, A. Kornowski, O. Benson, H. Weller, J. Phys. Chem. B 108 (2004) 18826.
[15] (a) P. Reiss, J. Bleuse, A. Pron, Nano Lett 2 (2002) 781;
(b) R.E. Bailey, S. Nie, J. Am. Chem. Soc. 125 (2003) 7100;
(c) X. Zhong, Y. Han, Z. Dong, T.J. White, W. Knoll, J. Am. Chem. Soc. 125 (2003) 8589.
[16] B.A. Korgel, H.G. Monbouquette, Langmuir 16 (2000) 3588.
[17] W. Wang, L. Germanenko, M.S. El-Shall, Chem. Mater. 14 (2002) 3028.
[18] D.V. Petrov, B.S. Santos, G.A.L. Pereira, C.D.M. Donega, J. Phys. Chem. B 106 (2002) 5325.

[19] N. Shailesh, Sharma, S. Zeena, P. Pillai, V. Kamat, J. Phys. Chem. B 107 (2003) 10088.

[20] H. Sharma, S.N. Sharma, G. Singh, S.M. Shivaprasad, Physica E 31 (2006) 180.

[21] J.A. Gaunt, A.E. Knight, S.A. Windsor, V. Chechik, J. Colloid Interface Sci. 290 (2005) 437.

[22] A.R. Kortan, R. Hull, R.L. Opila, M.G. Bawendi, M.L. Steigerwald, P.J. Caroll, L.E. Brus, J. Am. Chem. Soc. 112 (1990) 1327.

[23] V.V. Nikesh, S. Mahamuni, Semicond. Sci. Technol. 16 (2001) 687.

[24] G. Bhagavannarayana, N. Shailesh, R.K. Sharma, S.T. Sharma, Lakshmikumar, Mats. Chem. Phys. 97 (2006) 442.

[25] N. Shailesh, R.K. Sharma, S.T. Sharma, Lakshmikumar, Physica E 28 (3) (2005) 264.

[26] T.Y. Kim, J.Y. Kim, S.H. Lee, H.W. Shim, S.H. Lee, E.K. Suh, K.S. Nahm, Synth. Met. 144 (2004) 61.

[27] M. Azad, Malik, Neerish Revaprasadu, Paul O'Brien, Chem. Mater. 13 (2001) 913.

[28] Y.D. Kim, M.V. Klein, S.F. Ren, Y.C. Chang, H. Juo, N. Samarth, J.K. Furdyna, Phys. Rev. B: Condens. Matter 49 (1994) 7262.

[29] R. Hill, D. Richardson, Thin Solid Films 18 (1973) 25.

[30] R. Venugopal, P.-I. Lin, Y.-T. Chen, J. Phys. Chem. B 110 (2006) 11691.

[31] N. Benosman, N. Amrane, H. Aourag, Phys. B 275 (2000) 316.

[32] P. Gupta, B. Maiti, A.B. Maity, S. Chaudhuri, A.K. Pal, Thin Solid Films 260 (1995) 75.

[33] R. Hill, J. Phys. C: Solid State Phys. 7 (1974) 521.

[34] A. Etchberry, F. Iranzo-Marin, E. Novakovic, R. Triboulet, C. Debiemme-Chouvy, J. Cryst. Growth 184–185 (1998) 213.

[35] C.D. Wagner, W.M. Riggs, L.E. Davis, J.F. Moulder, Handbook of X-ray Photoelectron Spectroscopy, Perkin–Elmer Corporation, Eden Prairie, 1979.

[36] L. Manna, E.C. Scher, L.S. Li, A.P. Alivisatos, J. Am. Chem. Soc. 124 (2002) 7136.

[37] G.W. Huang, C.Y. Chen, K.C. Wu, M.O. Ahmed, P.T. Chou, J. Cryst. Growth 265 (2004) 250.